Available online at www.sciencedirect.com
ScienceDirect
Progress in Natural Science 18 (2008) 413–419
Progress in Natural Science
www.elsevier.com/locate/pnsc

Effects of zonal perturbations of sea surface temperature on tropical equilibrium states: A cloud-resolving modeling study

Xiaopeng Cui *, Shouting Gao

Laboratory of Cloud-Precipitation Physics and Severe Storms, Institute of Atmospheric Physics, Chinese Academy of Sciences, Beijing 100029, China

Received 18 June 2007; received in revised form 21 September 2007; accepted 15 October 2007

Abstract

The effects of zonal perturbations of sea surface temperature (SST) on tropical equilibrium states are investigated based on a series of two-dimensional cloud-resolving simulations with imposed zero vertical velocity, constant zonal wind, and a zonal model domain of 768 km. Four experiments with zonal SST perturbations of wavenumbers 1 (C1), 2 (C2), 4 (C3), and 8 (C4) are compared to a control experiment with zonally uniform SST (C0). The 40-day integrations show that the temperatures reach quasi-equilibrium states with distinct differences. C1 and C2 produce warmer equilibrium states whereas C3 and C4 generate colder equilibrium states than C0 does. The heat budgets in the five experiments are analyzed. Compared to C0, less IR cooling over smaller clear-sky regions in C1 and more condensational heating in C2 are responsible for warmer equilibrium states. A reduced condensational heating leads to the cold equilibrium state in C3. The interaction between convective systems in C4 causes a decrease of condensational heating, which accounts for the cold equilibrium state.

Keywords: Tropical equilibrium states; Sea surface temperature; Zonal perturbation; Cloud-resolving modeling study

Tropical climate may be affected by physical processes such as surface fluxes associated with sea surface temperature (SST), diurnal variations, and cloud-radiation interactions. The studies of physical processes controlling tropical equilibrium climate require numerical models that include detailed physical processes associated with individual cloud. Nakajima and Matsuno [1] used a two-dimensional (2D) cloud-resolving model with a constant radiative cooling profile and water microphysical schemes to study tropical cloud clusters. Their experiments with the 50-h integrations simulated tropical quasi-equilibrium states, which was the first successful experiment for equilibrium simulations. Similar equilibrium simulations have been conducted in a three-dimensional (3D) model with a constant radiative cooling [2] as well as in a 2D model with interactive cloud-radiative forcing, water, and ice microphysical schemes [3].

Lau et al. [4] and Sui et al. [5] (S94 hereafter) studied the tropical water and energy cycles and their roles in the tropical system by integrating the 2D cloud-resolving model to the climate equilibrium states. The model uses initial conditions from a 1956 Marshall Islands Experiment in the central Pacific and is imposed with a time-invariant horizontally-uniform large-scale vertical velocity and a fixed SST at 28 °C, in which the simulated atmosphere is conditionally unstable below the freezing level and close to neutral above the freezing level. After the adjustment in about 20 days, the simulations reached the quasi-equilibrium states with a temperature of 258 K and precipitable water of 51 mm. Grabowski et al. [6] (G96 hereafter) integrated the 2D cloud-resolving model for 24 days with similar initial conditions and found a quasi-equilibrium state

* Corresponding author. Tel.: +86 10 82995105; fax: +86 10 82995308.
E-mail address: xpcui@mail.iap.ac.cn (X. Cui).

1002-0071/$ - see front matter © 2007 National Natural Science Foundation of China and Chinese Academy of Sciences. Published by Elsevier Limited and Science in China Press. All rights reserved.
doi:10.1016/j.pnsc.2007.10.007

with a temperature of 263 K and precipitable water of 70 mm. Thus, tropical equilibrium states were warmer and more humid in G96 than in S94. Xu and Randall [7] showed that the simulated statistical equilibrium state was between the cold/dry regime in S94 and the warm/humid regime in G96 and found that statistical equilibrium states were more sensitive to the transient large-scale forcing than to the magnitude of the forcing. Xu and Randall compared the model differences between S94 and G96 and found that S94's model may be unable to maintain the initial wind profile reducing the surface wind speed and weakening surface evaporation.

Robe and Emanuel [8] used a 3D cloud-resolving model with a constant radiative cooling profile and water microphysical schemes to simulate a statistical equilibrium state. The simulation reached an equilibrium state due to the balance between the net upward mass flux by moist convection and the net radiative cooling. The cloud mass flux increased with increasing radiative cooling. The mean updraft velocity was independent of the strength of the radiative forcing. Tompkins and Craig [9] used a 3D cloud-resolving model with interactive cloud-radiative forcing as well as water and ice microphysical schemes and also simulated a statistical equilibrium state. After 30 days of integration, they found that the adjustment time scale could be different, for instance, vertical mass flux was adjusted to the equilibrium state much more quickly than thermodynamic variables did. Xu and Randall [10] carried out the sensitivity tests of quasi-equilibrium states to large-scale advective cooling and moistening and found that the time-varying large-scale forcing had no significant impact on the long-term behaviors whereas they affected short-term variations.

Tao et al. [11] further compared the models by S94 and G96 and found that the mass-weighted relative humidity was 10% higher in G96 than that in S94. The convective available potential energy (CAPE) in G96 was also larger than that of S94. The microphysical parameterization schemes, grid sizes, and domains between their models were quite different. To explain the differences of equilibrium states between S94 and G96, Tao et al. [11] conducted sensitivity tests with the 2D cloud-resolving model and found that the equilibrium states are not sensitive to the initial conditions whereas they are sensitive to the minimum surface speed prescribed in the calculation of surface fluxes. Determination of equilibrium thermodynamic states depends on the surface evaporation, where surface wind plays a central role. Small surface evaporation associated with weak surface winds produces a cold and dry equilibrium state whereas large evaporation associated with strong surface winds causes a warm and humid equilibrium state. Shie et al. [12] revealed that vertical wind shear, minimum surface wind speed in the calculations of surface fluxes, and radiation determine thermodynamic quasi-equilibrium states. Gao et al. [13] examined the effect of diurnal solar heating on quasi-equilibrium cloud-resolving simulations and found that the simulation with a time-invariant solar zenith angle produced a colder and drier equilibrium state than the simulation did with a diurnally varied solar zenith angle since the former simulation produces less solar heating, more condensation, and consumes more moisture than the latter simulation does.

SST is an important parameter that affects tropical convective development by determining surface evaporation flux as well as surface sensible flux. Lau et al. [14] compared the experiments with the same large-scale forcing but different SSTs and found that the increase in SST induced surface cooling by increasing surface evaporation and produced a 13% increase in surface precipitation. Wu and Moncrieff [15] integrated a 2D cloud-resolving model to thermodynamic equilibrium states with different spatially and temporally invariant SSTs and found that the SST variation has large impacts on the water vapor feedback and small impacts on the cloud feedback, radiation budget, and surface energy budget. Grabowski et al. [16] conducted quasi-equilibrium cloud-resolving simulations with a large domain size of 4000 km and a large-scale SST gradient and revealed that the inclusion of the interactive radiation calculations led to a significant modification of the large-scale circulation and caused a large impact on convection in both intensity and horizontal scale. Yano [17] showed that the amplitudes of the SST gradients did not determine the intensity of the large-scale circulation. Gao et al. [13] investigated the impacts of diurnal SST variation on quasi-equilibrium cloud-resolving simulations and found that the simulation with a diurnally-varied SST generated a colder equilibrium state than did the simulation with a time-invariant SST because the former simulation produces a colder temperature through less latent heating and more IR cooling than the latter simulation does. Cui and Li [18] analyzed the effects of SST variation on surface rainfall with equilibrium cloud-resolving simulation data and found that surface evaporation pumped water vapor into rainfall-free regions and the divergence transports the vapor from rainfall-free regions to rainfall regions, which supports the rainfall. SST affects surface rainfall through changing surface evaporation in rainfall-free regions.

SST over the western Pacific warm pool is mainly determined by ocean surface radiative and heat fluxes [19,20], which is largely contributed by solar radiative flux and latent heat flux. Thus, horizontal distributions of SSTs are much affected by clouds in both temporal and spatial distributions as indicated by Fig. 1. Fig. 1 shows weekly-mean SST distribution over the western Pacific warm pool, which is averaged using daily-mean SST data of 18–24 April 2003. The SST data are retrieved from NASA/Tropical Rainfall Measuring Mission (TRMM) Microwave Imager (TMI) radiometer with a 10.7 GHz channel [21]. The SST affects the atmosphere mainly through surface evaporation that is associated with the covariance between surface wind speed and the specific humidity minus SST-dependent saturated specific humidity. The spatial distribution of SST may have an impact on tropical equilibrium states even if the horizontal mean SSTs are similar.

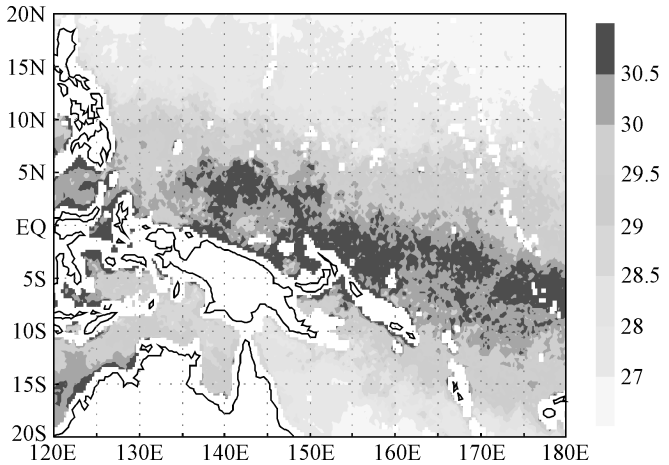

Fig. 1. Horizontal distribution of sea surface temperature averaged from the data of 18–24 April 2003 using TRMM TMI retrievals. Unit is in °C.

In this study, the sensitivity of tropical equilibrium states to zonal perturbations of SST was examined using a series of 2D cloud-resolving simulations. Four experiments imposed with idealized zonal SST distributions (zonal wavenumbers 1, 2, 4, and 8) were compared with the control experiment imposed with zonally-uniform SST.

1. Model and experimental design

The cloud-resolving model used in this study was originally developed by Soong and Ogura [22], Soong and Tao [23], and Tao and Simpson [24]. The 2D version of the model used by Sui et al. [5,25] and further modified by Li et al. [26] is what is used in this study. The governing equations and model setup can be found in Li et al. [26,27]. The model includes five prognostic equations for mixing ratios of cloud water, raindrop, cloud ice, snow, and graupel. The cloud microphysical parameterization schemes used in the model [26,27] are from Rutledge and Hobbs [28,29], Lin et al. [30], Tao et al. [31], as well as Krueger et al. [32]. The model also includes interactive solar [33] and thermal infrared [34,35] radiation parameterization schemes that are performed every 3 min. Cyclic lateral boundaries are used. At the top of the model, a free-slip condition is used for horizontal winds, temperature, and specific humidity, whereas zero vertical velocity is applied [24]. The horizontal domain is 768 km with a horizontal grid resolution of 1.5 km. The top model level is 42 mb. The vertical grid resolution ranges from about 200 m near the surface to about 1 km near 100 mb. The time step is 12 s. Hourly zonal-mean simulation data are used in the following analysis. The 2D cloud-resolving simulations have been validated with observations in terms of atmospheric thermodynamic profiles, surface fluxes, and surface rain rate in the tropics during TOGA COARE [26,36–40].

Due to a small model domain, the cloud-resolving model cannot simulate large-scale circulation. Thus, the large-scale forcing is imposed in the model to study the convective responses. To focus on the analysis of SST distribution on tropical equilibrium states, the model is forced by the zonally-uniform zero vertical velocity and a zonal wind of 4 m s^{-1}. Fig. 1 shows that over the western Pacific warm pool, small-scale SST signals have the spatial lengths of less than 1° longitude/latitude (100 km), which is associated with convective activity. Thus, the zonally-uniform SST of 29 °C and four harmonic components in the model domain (zonal wavenumbers 1, 2, 4, and 8 with the zonal scale of 768, 384, 192, and 96 km) (Fig. 2) are imposed in experiments C0, C1, C2, C3, and C4, respectively. The zonal SST perturbation can be ideally expressed by

$$\mathrm{SST}(x) = 29 - 0.5 \times \cos\left(\frac{2n\pi}{L}x\right) \quad (1)$$

where $L = 768$ km (zonal length of the 2D model domain); x is zonal distance; $n = 1, 2, 3, 4$ for C1, C2, C3, and C4, respectively. The amplitude of zonal SST perturbation is 1 °C. Note that the zonal-mean SST is 29 °C in five experiments. The vertical profiles of temperature and specific humidity averaged over the Intensive Flux Array (IFA) during TOGA COARE at 0400 LST 18 December 1992 [41] are used as the initial conditions. The model is integrated for 40.5 days for all five experiments.

2. Results

To examine the effects of zonal perturbation of SST on thermodynamic equilibrium, Fig. 3 shows the time series of daily-mean mass-weighted mean temperature and precipitable water (PW) in five experiments. During 40-day integrations, temperatures in all five experiments show quasi-equilibrium states with distinct differences (Fig. 3(a)) whereas PW does not display distinct equilibrium differences in the five experiments. Compared to C0 (−2.8 °C), the zonally-varied SST with zonal wavenumbers 4 (−4.5 °C) and 8 (−3.6 °C) produce colder equilibrium states whereas the zonally-varied SST with zonal wavenumbers 1 (−2.5 °C mm) and 2 (−2.3 °C) generates

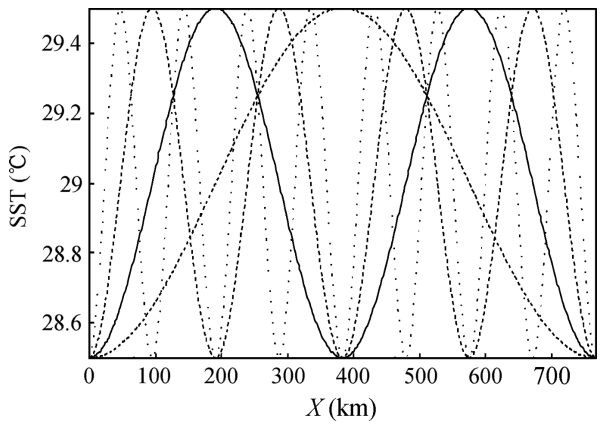

Fig. 2. Horizontal distributions of time-invariant sea surface temperatures (°C) in C0 (dark solid), C1 (dark dashed), C2 (solid), C3 (dashed), and C4 (dot).

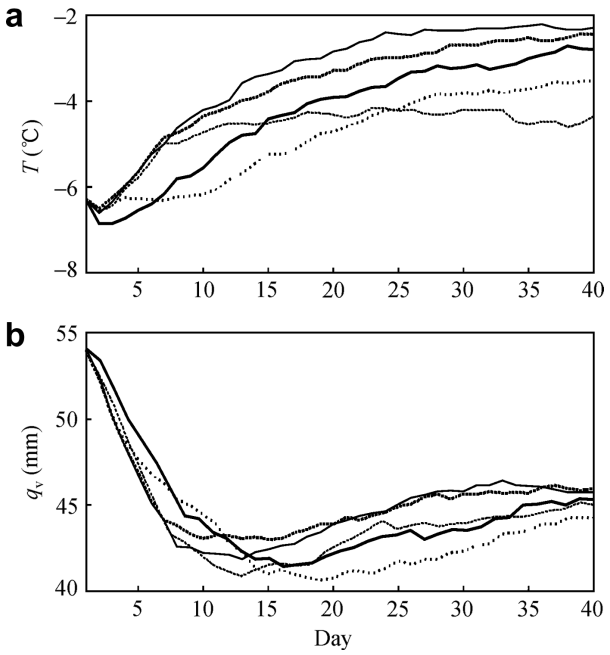

Fig. 3. Temporal evolution of (a) mass-weighted mean temperature (°C) and (b) precipitable water (mm) in C0 (dark solid), C1 (dark dashed), C2 (solid), C3 (dashed), and C4 (dot).

warmer equilibrium states. The analysis of additional sensitivity experiments indicates that the results are not affected by the model setups including zonal-mean SST, amplitude of zonal SST perturbation, and imposed vertical velocity and zonal wind.

To explain thermal equilibrium differences, the mass-weighted mean temperature budget is analyzed. Following Li et al. [26], zonal-mean heat budget can be expressed by

$$\frac{\partial\langle\overline{T}\rangle}{\partial t} = \frac{\langle\overline{Q}_{\mathrm{cn}}\rangle}{c_{\mathrm{p}}} + \frac{\langle\overline{Q}_{\mathrm{R}}\rangle}{c_{\mathrm{p}}} + \overline{H}_{\mathrm{s}} \tag{2}$$

Here, $\langle()\rangle = \frac{[()]}{[1]}$, $[()](=\int_0^{z_t}()\bar{\rho}\,\mathrm{d}z$, and z_t is the model top) is a mass integration; u and w are zonal and vertical air wind components, respectively; θ and q_{v} are air potential temperature and specific humidity, respectively; $\pi = (p/p_o)^{\kappa}$, $\kappa = R/c_{\mathrm{p}}$, R is the gas constant, c_{p} is the specific heat of dry air at constant pressure p, and $p_o = 1000$ hPa; $\bar{\rho}$ is a mean air density, which is a function of height only; Q_{cn} denotes the net latent heat release; Q_{R} is the radiative heating rate due to convergence of net flux of solar and infrared radiative fluxes; H_{s} is surface-sensible heat flux; a variable F with overbar ($\overline{F}$) is the zonal mean over the cyclic model domain. Eq. (2) states that the local temperature change is determined by condensational heating, radiative heating, and surface-sensible heat flux.

Fig. 3 shows that C4 and C3 reduce their warming trends on day 4 and 8, respectively, eventually causing cold equilibrium states in C3 and C4 whereas C0, C1, and C2 continue their warming courses. To explain physical processes that are responsible for thermal equilibrium states, the temperature budgets in five experiments are averaged over days 4–7 (Table 1), and the differences in temperature budgets for C1–C0, C2–C0, C3–C0, and C4–C0 are also calculated. The analysis on days 4–7 shows that the positive difference in temperature tendency is mainly determined by the positive difference in radiative heating for C1–C0. Fractional coverage for clear-sky regions is 56.9% in C0 (Fig. 4(a)) with a uniform SST of 29 °C over the model domain. Fractional coverage for clear-sky regions in C1 is 49.3% (Fig. 4(b)) since C1 has a 50% of the model domain where it is colder than 29 °C and convection is suppressed. The positive difference in radiative heating for C1–C0 is determined by the positive difference in IR cooling over clear-sky regions (Table 2) due to the fact that C1 has a smaller clear-sky area than C0 does. The convection is more organized in C1 than in C0 (Fig. 4(a) and (b)). As a result, both experiments exhibit similar contributions from condensational heating to temperature tendency.

Table 1 reveals that the positive differences in temperature tendencies for C2–C0 and C3–C0 are mainly caused by the positive differences in condensational heating during days 4–7. Although convection occupies similar sizes of areas in C0 (43.1%), C2 (45.8%), and C3 (42.8%), the convection in C2 and C3 (Fig. 4(c) and (d)) is more organized than in C0, explaining that more condensational heating occurs in C2 and C3 than in C0. Meanwhile, the similar sizes of clear-sky regions in C0 (56.9%), C2 (54.2), and C3 (57.2) significantly reduce the difference in IR cooling over clear-sky regions, which causes small contributions to the positive differences in temperature tendencies for C2–C0 and C3–C0.

The negative difference in temperature tendency is mainly caused by the negative difference in condensational heating for C4–C0 (Table 1). Since the distances between maximum SSTs are only 96 km in C4, convective systems interact with each other so that some convective systems are suppressed (e.g., around 140, 240, 355, 625, and 730 km) whereas other convective systems (e.g., around 50 and 430 km) cannot grow freely due to the limited areas of warm SST. As a result, the contribution from condensational heating to temperature tendency in C4 is smaller

Table 1
Zonal–mean mass-weighted mean temperature budgets (°C day^{-1}) in five experiments and temperature budget differences for C1–C0, C2–C0, C3–C0, and C4–C0 based on the data averaged from days 4 to 7

	C0	C1 (C1–C0)	C2 (C2–C0)	C3 (C3–C0)	C4 (C4–C0)
Temperature tendency	0.166	0.302 (0.136)	0.370 (0.204)	0.309 (0.143)	0.012 (−0.154)
Condensational heating	1.174	1.187 (0.013)	1.311 (0.137)	1.297 (0.123)	1.053 (−0.121)
Radiative heating	−0.986	−0.862 (0.124)	−0.919 (0.067)	−0.963 (0.023)	−1.016 (−0.030)
Surface-sensible heat flux	−0.022	−0.024 (−0.002)	−0.022 (0.000)	−0.024 (−0.002)	−0.024 (−0.002)

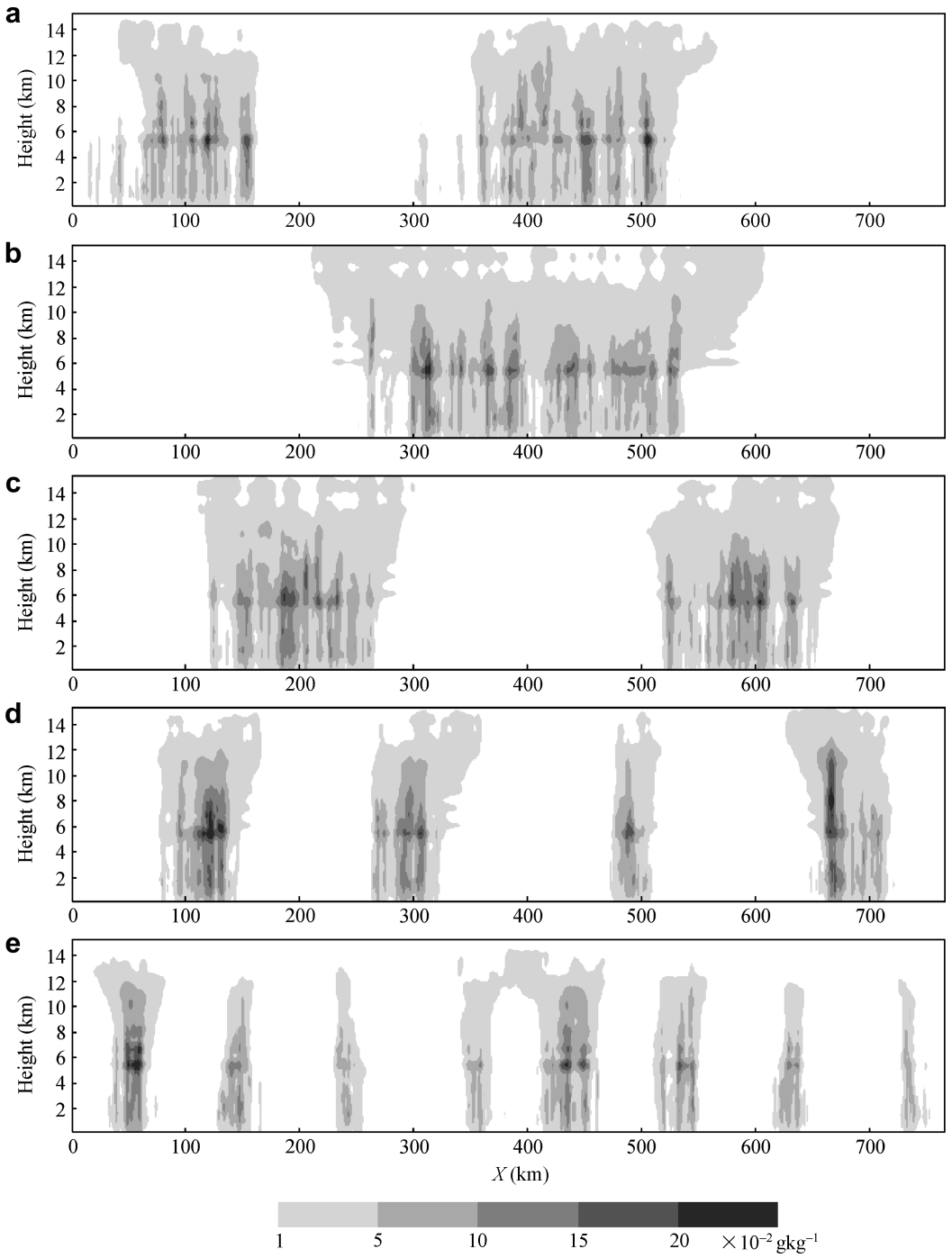

Fig. 4. Zonal–vertical (X–Z) cross sections of sum of the mixing ratios of hydrometeors (10^{-2} g kg^{-2}) averaged from days 4 to 7 in (a) C0, (b) C1, (c) C2, (d) C3, and (e) C4.

than in C0 (Table 1). Again, similar sizes of clear-sky regions in C0 (56.9%) and C4 (58.1) as well as cloudy regions in C0 (43.1%) and C4 (41.9%) cause a small difference in IR cooling over clear-sky regions and cloudy regions, which accounts for small contributions from IR cooling to the positive difference in temperature tendency for C4–C0.

The heat budgets averaged from days 4 to 7 are compared with those averaged from days 8 to 11 in C0–C3 (Table 3) to explain why C3 stops a warming course around day 8 that eventually leads to a cold equilibrium state (see Fig. 3). While C0 has a positive difference in temperature tendency between averages in days 8–11 and days 4–7, C1–C3 show negative differences and C3 has the largest negative difference (Table 3). This shows that C3 turns out to have a colder equilibrium state than C0 does (Fig. 3). The positive difference in temperature tendency in C0 is mainly determined by the positive difference in

Table 2
Temperature tendency differences in zonal-mean solar heating and IR cooling and corresponding contributions from clear-sky regions and cloudy regions for C1–C0, C2–C0, C3–C0, and C4–C0 based on the data averaged from days 4 to 7

	C1–C0	C2–C0	C3–C0	C4–C0
Zonal-mean solar heating	−0.015	−0.011	−0.011	0.000
Zonal-mean IR cooling	0.139	0.077	0.034	−0.030
Solar heating in clear-sky regions	−0.063	−0.029	−0.013	0.000
IR cooling in clear-sky regions	0.134	0.045	0.000	0.004
Solar heating in cloudy regions	0.048	0.018	0.002	0.000
IR cooling in cloudy regions	0.005	0.032	0.034	−0.034

Unit is in °C day^{-1}.

Table 4
Temperature tendency differences in zonal-mean solar heating and IR cooling and corresponding contributions from clear-sky regions and cloudy regions for C0–C3 between averages in days 8–11 and days 4–7

	C0	C1	C2	C3
Zonal-mean solar heating	−0.017	0.001	−0.009	−0.006
Zonal-mean IR cooling	0.141	−0.002	0.058	−0.006
Solar heating in clear-sky regions	−0.080	−0.041	−0.076	−0.052
IR cooling in clear-sky regions	0.200	0.161	0.230	0.135
Solar heating in cloudy regions	0.063	0.042	0.067	0.046
IR cooling in cloudy regions	−0.059	−0.163	−0.172	−0.141

Unit is in °C day^{-1}.

radiative heating. The negative differences in temperature tendency in C1–C3 are determined by the negative differences in condensational heating and C2 has the largest negative difference. The positive difference in radiative heating offsets the negative difference in condensational heating in C2, thereby decreasing the magnitude of the negative difference in temperature tendency. The negative difference in radiative heating along with the negative difference in condensational heating in C3 serves to increase the magnitude of the negative difference in temperature tendency. The shrinking of zonal areas of tropical water clouds in C1–C3 reduce the vapor condensation and associated condensational heating in days 8–11, compared to those in days 4–7 (not shown). Further analysis (Table 4) reveals that the positive differences in radiative heating in C0 and C2 are caused by the positive difference in IR cooling over clear-sky regions. The small differences in radiative heating in C1 and C3 are from the cancellation in solar heating and IR cooling over clear-sky regions and cloudy regions, respectively. The positive differences in radiative heating in C0 and C2 may be the results of significant reductions of clear-sky regions from days 4 to 7 (56.9% in C0 and 54.2% in C2) to days 8–11 (48.3% in C0 and 44.8% in C2).

3. Conclusion

The effects of zonal perturbations of sea surface temperature (SST) on tropical equilibrium states are investigated with a series of two-dimensional cloud-resolving simulations. The experiments (C1, C2, C3, and C4) with zonally varied SST with zonal wavenumbers 1, 2, 4, and 8 (zonal scales of 768, 384, 192, and 96 km) are compared to the experiment with zonally uniform SST (C0). The model is integrated for about 40 days in the framework of zero-imposed vertical velocity and constant westerly wind.

The temperature equilibrium states show distinct differences in the five experiments whereas precipitable water equilibrium states do not. Compared to C0, C1 and C2 produce warmer equilibrium states whereas C3 and C4 generate colder equilibrium states. Mass-weighted mean temperature budgets in the five experiments are calculated to explain the dominant physical processes that are responsible for these thermal equilibrium differences. C1 has a wavenumber 1 distribution of SST that leads to less than 50% of the model domain for clear-sky regions. The zonal gradient of SST regulates a strong convective system whereas C0 has no zonal gradient of SST and instead has a loose convective system with more than 50% of clear-sky regions. As a result, C1 has a warmer equilibrium state than C0 because C1 has less IR cooling over smaller clear-sky regions than C0. C2 produces a warmer equilibrium state than C0 does since C2 has more condensational heating associated with more organized convection than C0. C3 stops a warming trend around day 8 and eventually has a colder equilibrium state, compared to C0. This is due to the fact that C3 generates less condensational heating associated with the shrink of zonal area of water clouds after day 8 than before and radiative heating does not show any significant differences before or after day 8. C4 slows down the warming after day 4 and it has a colder equilibrium state than C0 at the end of integrations. Convective systems associated with warm SSTs interact with each other since they are only 96 km apart in C4. This interaction suppresses some convective systems whereas other convective systems cannot grow freely due to the limited area of warm SSTs, which leads to the weakening of condensational heating. Thus, the reduced condensational heating in C4 is responsible for the colder equilibrium state.

Table 3
Zonal–mean mass-weighted mean temperature budgets (°C day^{-1}) averaged from days 8 to 11 in C0–C3 and differences (brackets) in temperature budgets between averages from days 8 to 11 and days 4 to 7

	C0	C1	C2	C3
Temperature tendency	0.233 (0.067)	0.132 (−0.170)	0.196 (−0.174)	0.103 (−0.206)
Condensational heating	1.125 (−0.049)	1.017 (−0.170)	1.087 (−0.224)	1.103 (−0.194)
Radiative heating	−0.862 (0.124)	−0.864 (−0.002)	−0.871 (0.048)	−0.974 (−0.011)
Surface-sensible heat flux	−0.029 (−0.007)	−0.022 (0.002)	−0.021 (0.001)	−0.026 (−0.002)

Acknowledgments

This work was supported by National Natural Science Foundation of China (Grant No. 40505012), the '100 Talents Project' of Chinese Academy of Sciences (Grant No. KCL14014), the Knowledge Innovation Program of the Chinese Academy of Sciences (IAP07214) and "Outstanding Oversea Scholars" (Grant No. 2005-2-17).

References

[1] Nakajima K, Matsuno T. Numerical experiments concerning the origin of cloud clusters in the tropical atmosphere. J Meteor Soc Japan 1988;66:309–29.
[2] Islam S, Bras RL, Emanuel KA. Predictability of mesoscale rainfall in the tropics. J Appl Meteor 1993;32:297–310.
[3] Held IM, Hemler RS. Radiative–convective equilibrium with explicit two-dimensional moist convection. J Atmos Sci 1993;50:3909–27.
[4] Lau KM, Sui CH, Tao WK. A preliminary study of the tropical water cycle and its sensitivity to surface warming. Bull Amer Meteor Soc 1993;74:1313–21.
[5] Sui CH, Lau KM, Tao WK, et al. The tropical water and energy cycles in a cumulus ensemble model. Part I. Equilibrium climate. J Atmos Sci 1994;51:711–28.
[6] Grabowski WW, Moncrieff MW, Kiehl JT. Long-term behaviour of precipitating tropical cloud systems: a numerical study. Quart J Roy Meteor Soc 1996;122:1019–42.
[7] Xu KM, Randall DA. A sensitivity study of radiative–convective equilibrium in the tropics with a convection-resolving model. J Atmos Sci 1999;56:3385–99.
[8] Robe FR, Emanuel KA. Moist convective scaling: some inferences from three-dimensional cloud ensemble simulations. J Atmos Sci 1996;53:3265–75.
[9] Tompkins AM, Craig GC. Radiative-convective equilibrium in a three-dimensional cloud-ensemble model. Quart J Roy Meteor Soc 1998;124:2073–97.
[10] Xu KM, Randall DA. Influence of large-scale advective cooling and moistening effects on the quasi-equilibrium behavior of explicitly simulated cumulus ensembles. J Atmos Sci 1998;55:896–909.
[11] Tao WK, Simpson J, Sui CH, et al. Equilibrium states simulated by cloud-resolving models. J Atmos Sci 1999;56:3128–39.
[12] Shie CL, Tao WK, Simpson J, et al. Quasi-equilibrium states in the tropics simulated by a cloud-resolving model. Part I. Specific features and budget analysis. J Climate 2003;16:817–33.
[13] Gao S, Zhou Y, Li X. Effects of diurnal variations on tropical equilibrium states: a two-dimensional cloud-resolving modeling study. J Atmos Sci 2007;64:656–64.
[14] Lau KM, Sui CH, Chou MD, et al. An inquiry into the cirrus cloud thermostat effect for tropical sea surface temperature. Geophys Res Lett 1994;21:1157–60.
[15] Wu X, Moncrieff MW. Effects of sea surface temperature and large-scale dynamics on the thermodynamic equilibrium state and convection over the tropical western Pacific. J Geophys Res 1999;104:6093–100.
[16] Grabowski WW, Yano JI, Moncrieff MW. Cloud resolving modeling of tropical circulations driven by large-scale SST gradients. J Atmos Sci 2000;57:2022–39.
[17] Yano JI, Grabowski WW, Moncrieff MW. Mean-state convective circulations over large-scale tropical SST gradients. J Atmos Sci 2002;59:1578–92.
[18] Cui X, Li X. Role of surface evaporation in surface rainfall processes. J Geophys Res 2006;111:D17112. doi:10.1029/2005JD006876.
[19] Li X, Sui CH, Adamec D, et al. Impacts of precipitation in the upper ocean in the western Pacific warm pool during TOGA COARE. J Geophys Res 1998;103:5347–59.
[20] Sui CH, Li X, Rienecker MM, et al. The impacts of daily surface forcing in the upper ocean over tropical Pacific: a numerical study. J Climate 2003;16:756–66.
[21] Wentz FJ, Gentemann C, Smith D, et al. Satellite measurements of sea surface temperature through clouds. Science 2000;288:847–50.
[22] Soong ST, Ogura Y. Response of tradewind cumuli to large-scale processes. J Atmos Sci 1980;37:2035–50.
[23] Soong ST, Tao WK. Response of deep tropical cumulus clouds to mesoscale processes. J Atmos Sci 1980;37:2016–34.
[24] Tao WK, Simpson J. The Goddard Cumulus Ensemble model. Part I. Model description. Terr Atmos Oceanic Sci 1993;4:35–72.
[25] Sui CH, Li X, Lau KM. Radiative-convective processes in simulated diurnal variations of tropical oceanic convection. J Atmos Sci 1998;55:2345–59.
[26] Li X, Sui CH, Lau KM, et al. Large-scale forcing and cloud-radiation interaction in the tropical deep convective regime. J Atmos Sci 1999;56:3028–42.
[27] Li X, Sui CH, Lau KM. Dominant cloud microphysical processes in a tropical oceanic convective system: a 2-D cloud resolving modeling study. Mon Wea Rev 2002;130:2481–91.
[28] Rutledge SA, Hobbs PV. The mesoscale and microscale structure and organization of clouds and precipitation in midlatitude cyclones. Part VIII. A model for the "seeder-feeder" process in warm-frontal rainbands. J Atmos Sci 1983;40:1185–206.
[29] Rutledge SA, Hobbs PV. The mesoscale and microscale structure and organization of clouds and precipitation in midlatitude cyclones. Part VIII. A model for the "seeder-feeder" process in warm-frontal rainbands. J Atmos Sci 1984;41:2949–72.
[30] Lin YL, Farley RD, Orville HD. Bulk parameterization of the snow field in a cloud model. J Climate Appl Meteor 1983;22:1065–92.
[31] Tao WK, Simpson J, McCumber M. An ice–water saturation adjustment. Mon Wea Rev 1989;117:231–5.
[32] Krueger SK, Fu Q, Liou KN, et al. Improvement of an ice-phase microphysics parameterization for use in numerical simulations of tropical convection. J Appl Meteor 1995;34:281–7.
[33] Chou MD, Suarez MJ, Ho CH, et al. Parameterizations for cloud overlapping and shortwave single scattering properties for use in general circulation and cloud ensemble models. J Atmos Sci 1998;55:201–14.
[34] Chou MD, Kratz DP, Ridgway W. Infrared radiation parameterization in numerical climate models. J Climate 1991;4:424–37.
[35] Chou MD, Suarez MJ. An efficient thermal infrared radiation parameterization for use in general circulation model. NASA Tech. Memo. 104606, vol. 3, 1994. p. 85. Available from: NASA/Goddard Space Flight Center, Code 913, Greenbelt, MD 20771.
[36] Gao S, Cui X, Zhu Y, et al. Surface rainfall processes as simulated in a cloud resolving model. J Geophys Res 2005;110:D10202. doi:10.1029/2004JD005467.
[37] Gao S, Cui X, Zhou Y, et al. A modeling study of moist and dynamic vorticity vectors associated with 2D tropical convection. J Geophys Res 2005;110:D17104. doi:10.1029/2004JD005675.
[38] Gao S, Ping F, Li X. Cloud microphysical processes associated with the diurnal variations of tropical convection: a 2D cloud resolving modeling study. Meteor Atmos Phys 2006;91:9–16.
[39] Gao S, Ran L, Li X. Impacts of ice microphysics on rainfall and thermodynamic processes in the tropical deep convective regime: a 2D cloud-resolving modeling study. Mon Wea Rev 2006;134:3015–24.
[40] Gao S, Ping F, Cui X, et al. Short timescale air–sea coupling in the tropical deep convective regime. Meteor Atmos Phys 2006. doi:10.1007/s00703-005-0161-8.
[41] Sui CH, Lau KM, Takayabu Y, et al. Diurnal variations in tropical oceanic cumulus ensemble during TOGA COARE. J Atmos Sci 1997;54:639–55.